

Cycle-by-cycle analysis of cold crank-start in a GDI engine

Author, co-author (Do NOT enter this information. It will be pulled from participant tab in MyTechZone)

Affiliation (Do NOT enter this information. It will be pulled from participant tab in MyTechZone)

Abstract

The first 3 cycles in the cold crank-start process at 20°C are studied in a GDI engine. The focus is on the dependence of the HC and PM/PN emissions of each cycle on the injection strategy and combustion phasing of the current and previous cycles. The PM/PN emissions per cycle decrease by more than an order of magnitude as the crank-start progresses from the 1st to the 3rd cycle, while the HC emissions stay relatively constant. The wall heat transfer, as controlled by the combustion phasing, during the previous cycles has a more significant influence on the mixture formation process for the current cycle than the amount of residual fuel. The results show that the rise in HC emissions caused by the injection spray interacting with the intake valves and piston crown is reduced as the cranking process progresses. Combustion phasing retard significantly reduces the PM emission. The HC emissions, however, are relatively not sensitive to combustion phasing in the range of interest.

Introduction

In response to growing concerns over global warming and climate change, the CO₂ emissions legislations around the world have become increasingly stringent. Figure 1 shows the evolution of the CO₂ legislation for light duty vehicles (LDV) in different parts of the world as they strive towards a goal of approximately 100 grams of CO₂ per kilometer during the next decade.

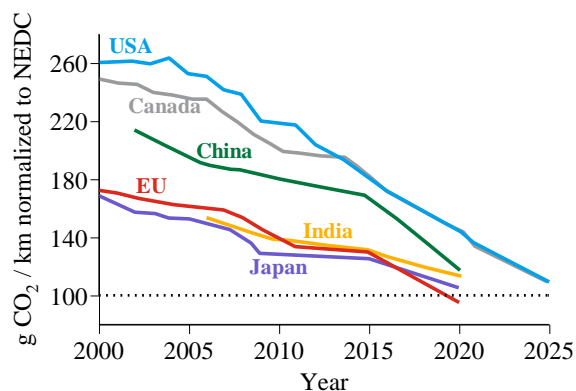


Figure 1. Light duty vehicles CO₂ emissions regulations around the world. Data normalized to NEDC. Adapted from [1]

The tightening of the fuel consumption standards has been a driver for the adoption of new technologies during the past decade; among them gasoline direct injection (GDI) engines. According to EPA and NHTSA estimates [2], downsized turbocharged GDI engines with cooled EGR have a potential for CO₂ emissions reduction between 16% and 25% compared to the 2008 gasoline engine (PFI, NA) used as a baseline. As this potential has been tapped during the past decade the market penetration of GDI engines has grown at an accelerated pace (see Fig. 2). Despite the advantages in fuel consumption of GDI engines, the liquid fuel injection into the combustion chamber poses emissions challenges, particularly during the cold-start phase where over 95% of the HC [5] and over 75% of the PM/PN [6] tailpipe emissions take place.

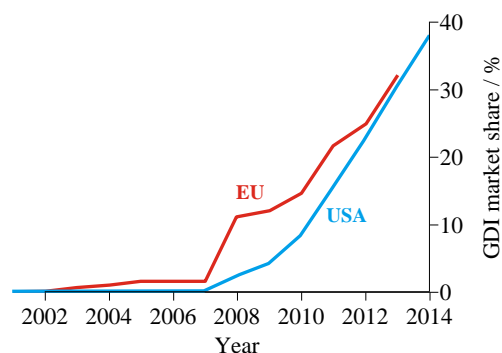


Figure 2. Market penetration of GDI engines in the US and the EU for the past decade. Data source: US [3]; EU [4]

Figure 3 shows the engine behavior during a typical cold crank-start of a GDI engine. Prior to the first combustion cycle the engine is driven by the starter motor at approximately 280 rpm. After the 1st combustion event the engine speed increases rapidly and reaches its maximum speed (a.k.a. speed flare) within 1 second. After the speed flare, the engine speed decreases to the targeted cold fast-idle speed. As can be seen from the cumulative engine out emissions in Fig. 4, the engine cold crank-start is responsible for a disproportionate amount of the cold-start phase emissions. During the initial 4 seconds (0.2% of the total FTP-75 duration) 110 mg of HC and 5 mg of PM were emitted, corresponding to 32% and 15% of the T3B50 limit respectively.

In comparison to all the other operation points during the certification driving cycle, the cold crank-start is subject to the lowest temperature and lowest engine speed. As a result, the fuel evaporation and mixture formation process are compromised and significant over-fueling is necessary to produce an ignitable fuel-air mixture. Because of the large

amount of fuel injected, a significant portion of the injected fuel lands on the cold combustion chamber surfaces, resulting in fuel films that fail to evaporate before combustion. Optical investigations conducted by Costanzo et al. [7] provide evidence of the significant role that these fuel films play on HC emissions and PM formation. Additionally, the low temperature impacts negatively the classical HC emissions mechanisms identified by Cheng et al. [8]; low temperature results in larger crevice volumes, increases the solubility of hydrocarbons into the lubricant oil layer, and intensifies the heat transfer rates from the hot gases into the cylinder walls. The latter increases the flame quenching distance and reduces the post-flame oxidation rate of the resulting pollutants after combustion.

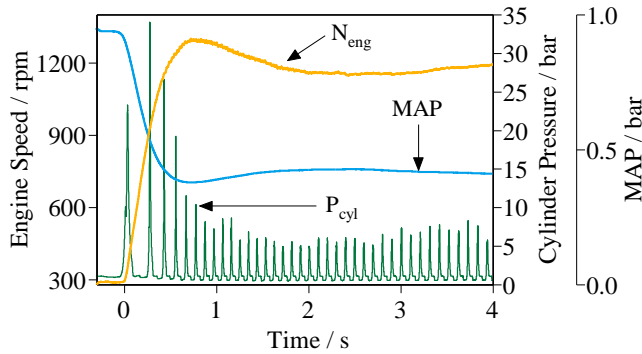


Figure 3. Cylinder pressure, engine speed and intake manifold pressure traces during cold crank-start.

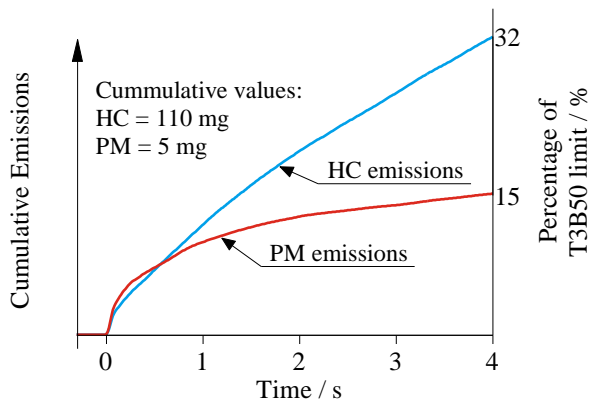


Figure 4. Cold crank-start cumulative emissions as percentage of the T3B50/ULEV50 limit [9]. The HC limit of T3B50 assumes the same HC/NOx ratio as the T2B5 standard

This study seeks to expand the understanding of the HC and PM/PN emissions behavior during the cold crank-start process of a GDI engine. For that purpose the initial 3 engine cycles are analyzed individually under a set of parameters that include the mass of injected fuel, the start of injection (SOI), and the ignition timing. Additionally, the interactions between cycles are also considered by studying the impact that the heat transfer history and the residual fuel from previous injection events have on the mixture formation and fuel enrichment requirement of the current cycle.

The research presented on this paper is a natural extension of previous studies by the authors focusing on 1st cycle emissions and fuel pathway during cold crank-start [9, 10]. This study also builds upon the methodology developed at the Sloan Automotive Laboratory at MIT for experimentally studying the first combustion cycle and the cranking process in PFI engines [11, 12, 13, 14, 15, 16, 17].

Experimental Methodology

Engine set up

The experiments were carried out using a commercial 4-cylinder, 2 liter GDI engine featuring side-mounted electromagnetic injectors, with a 52° cone angle, a 25° inclination from the horizontal and 6 holes. The variable valve timing (VVT) system was deactivated and a fixed valve timing was used for all of the experiments (see Table 1).

Table 1. Specifications of the GM – LNF engine

| | |
|----------------------------|---------------------------------|
| Displacement | 1998 cc |
| Bore / Stroke | 86 / 86 mm |
| Connecting Rod | 145.5 mm |
| Compression ratio | 9.2:1 |
| Fuel pressure | 50 bar |
| Intake Valve Open / Close | 11°aTDC / 61°aBDC @ 0.2 mm lift |
| Max. intake valve lift | 10.3 mm @ 126°aTDC |
| Exhaust Valve Open / Close | 52°bBDC / 10°bTDC @ 0.2 mm lift |
| Max. exhaust valve lift | 10.3 mm @ 125°aTDC |

In real GDI applications the typical fuel pressure for the initial injection events during cranking ranges between 30 and 70 bar [18, 19] and is heavily dependent on engine speed. In the experimental setup used in this study, the fuel pressure was kept independent from engine operation and was maintained at a constant value of 50 bar by a hydro-pneumatic accumulator (see Fig. 6). A Tier II EEE certification gasoline was used with a carbon mass fraction of 86.5%, 29% aromatics content and a Reid vapor pressure of 62.7 kPa. The distillation curve can be found in Fig. 5. Three independent chillers for the fuel, intake air, engine oil and coolant were used to keep the cold crank-start conditions, with all temperatures at 20°C.

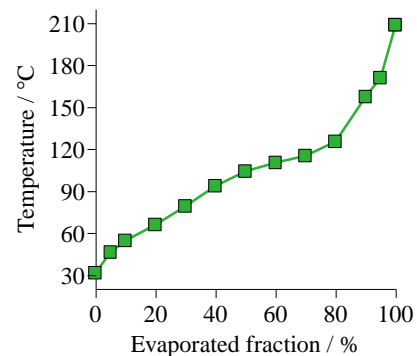


Figure 5. Distillation curve of the used Tier II EEE certification gasoline

The pollutant emissions were monitored at the exhaust runner of cylinder 4 using fast response analyzers. The wet HC mole fraction was measured by a fast FID (Cambustion HFR400) with a 10 to 90% time response of 1 ms. The CO and CO₂ wet mole fractions were measured by a fast NDIR (Cambustion NDIR500) with a 10 to 90% time response of 8 ms. Lastly, the particulate spectrum was measured using a differential mobility spectrometer (Cambustion DMS500) with a size range of 5-1000 nm and a 10 to 90% response of 300 ms.

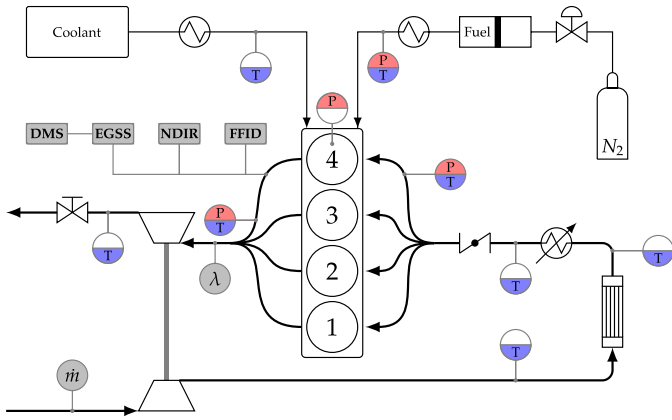


Figure 6. Diagram of the experimental setup and the sensor locations

In comparison to the fast FID and fast NDIR analyzers, the time response of the DMS is two orders of magnitude slower, precluding crank-angle resolved measurements of the particle spectrum. Still, at $t_{10-90\%} = 300$ ms, the instrument's response time is sufficient to allow cycle-resolved measurement. However, as the engine speed increases during crank-start, the time interval between two consecutive exhaust events might not be long enough to allow the DMS to completely differentiate between the emissions of two adjacent engine cycles. To overcome this obstacle for performing a cycle-resolved analysis of the initial 3 cycles, an exhaust gas sampling system (EGSS) is used.

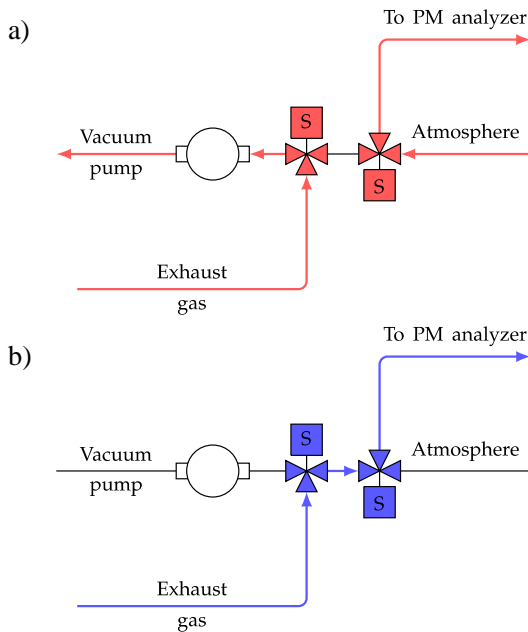


Figure 7. Exhaust gas sampling system (EGSS) for cycle-resolved particle spectrum measurement. a) Closed position feeds ambient air to the analyzer and circulates the exhaust gases to minimize the dead volume. b) Open position feeds exhaust sample to the analyzer

The objective of the EGSS is to supply to the analyzer only the exhaust gases from the desired cycle, while blocking the exhaust gases from previous and following cycles. The EGSS is located upstream of the DMS (Fig. 6) and consists of two three-way solenoid valves connected in series. In the “closed” position (Fig. 7-a), the exhaust gas is

circulated around the system by a rotary vane vacuum pump to in order to minimize dead volumes, while the DMS is allowed to sample ambient air in order to maintain its internal pressure within range. In the “open” position (Fig. 7-b) the exhaust and sample flows are connected, and the DMS is able to perform the particle spectrum measurement for the desired engine cycle. The solenoid valves have a 3/32” orifice and an opening time of 10 ms, which is fast enough to capture the exhaust flow period of 30 – 100 ms. The EGSS is controlled by a programmable microcontroller that uses the crankshaft encoder signal as an input for the timely triggering of the solenoid valves.

The emission values reported in this paper are presented in terms of mass per cylinder per cycle. Due to the transient nature of the experiments, it is difficult to measure the time-resolved exhaust flow rate using an air-flow meter. Instead, the in-cylinder pressure during the exhaust stroke was used to calculate the exhaust mass flow rate. The latter was then integrated with the concentration measurements over the exhaust stroke. Further details on the methodology used to convert the mole fraction and concentration values to mass emissions per cycle can be found in Ref. [9].

Experiment description

As pointed out in the experimental layout description (see Fig. 6), the study was done via cylinder #4 with the engine operating in single-cylinder mode. A direct consequence of this approach is the inability to achieve a speed transient that is representative of a 4-cylinder engine during crank-start. To circumvent this, the engine was torque-assisted by a 10hp electric motor during the simulated crank-start experiments. The motor control and speed-ramp were adjusted to achieve similar speed traces between multi-cylinder and single-cylinder crank-start (Fig. 8).

In all cases, an experimental run started with the engine motoring at cranking speed while the temperatures and the exhaust HC background concentration were monitored until steady state condition was achieved. After the steady-state motoring, and depending on the engine cycle of interest, one, two or three combustion events took place in cylinder 4 (see Fig. 8 a-c). Thereafter, engine was motored at a fixed speed for 50 additional engine cycles while the exhaust flow composition and temperatures were recorded. The engine was brought again to cranking-speed motoring until the purging of residual HC was completed and the steady-state condition was attained. Five experiments were performed for each experimental condition; the average values are reported.

Table 2. Operation parameters for the 1st, 2nd, and 3rd cycles

| Parameter | 1 st cycle | 2 nd cycle | 3 rd cycle |
|---|-----------------------|-----------------------|-----------------------|
| Engine speed / rpm | 280 | 800 | 1050 |
| MAP (mbar) | 900 | 750 | 600 |
| Fuel mass (FEF=1) / mg | 29.5 | 26 | 21 |
| FEF / - | 1.7 ... 3.3 | 1.5 ... 2.1 | 1.3 ... 1.9 |
| SOI / °CA aTDC _{intake} | 45 ... 315 | 45 ... 315 | 45 ... 315 |
| Spark timing / °CA aTDC _{comp} | -45 ... 5 | -45 ... 5 | -45 ... -5 |

Throughout all of the experiments the throttle opening was fixed at the fast-idle position (2 bar NIMEP, 1200 rpm). The engine operated in the open-loop mode with the fuel amount being a function of the

demanded enrichment, the engine speed and the intake manifold pressure (speed-density calibration). Table 2 contains a summary of the typical values of the relevant parameters for the initial 3 engine cycles.

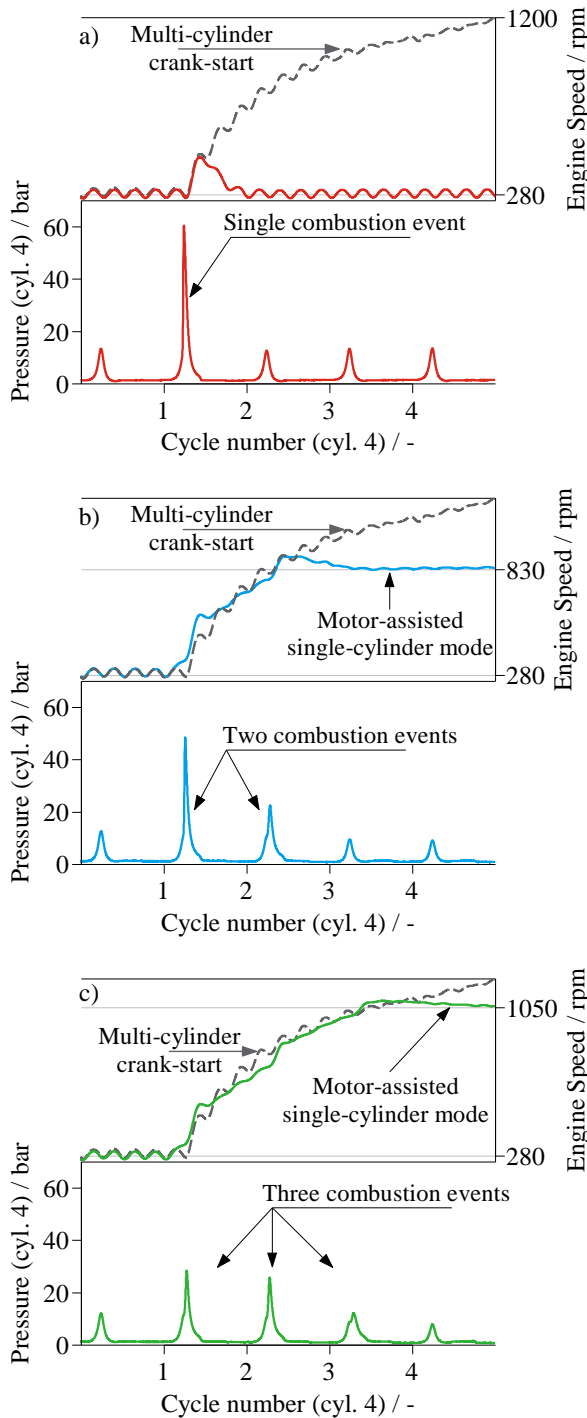


Figure 8. Representative engine speed and pressure traces for the 1st (a), 2nd (b), and 3rd (c) cycle experiments

Results and discussion

The results contained in this section deal with the effects of different parameters on the HC and PM/PN emissions performance of the initial 3 cycles during cold crank-start. The parameters studied are the spark timing, start of injection (SOI), and the *fuel enrichment factor* (FEF). The FEF is a dimensionless parameter used to quantify the fuel mass injected compared to the amount of fuel required to form a stoichiometric mixture with the inducted air; it is defined as follows:

$$FEF = \frac{m_{f,cyl}}{V_{cyl} \cdot \eta_{vol} \cdot \rho_{int} \cdot (F/A)_{stoich}} \quad (1)$$

The volumetric efficiency η_{vol} is referenced to the intake manifold condition; it is calibrated by motoring at steady state with the same engine speed as the instantaneous value during cranking.

Fuel enrichment factor effect

1st cycle of cranking dependence on FEF_{1st}

The impact of the FEF_{1st} on the 1st cycle HC and PM emissions has been covered in detail in a previous publication by the authors [9]. It is discussed here in connection to the 2nd cycle of cranking. Some of the most important results and trends are shown in Fig 9.

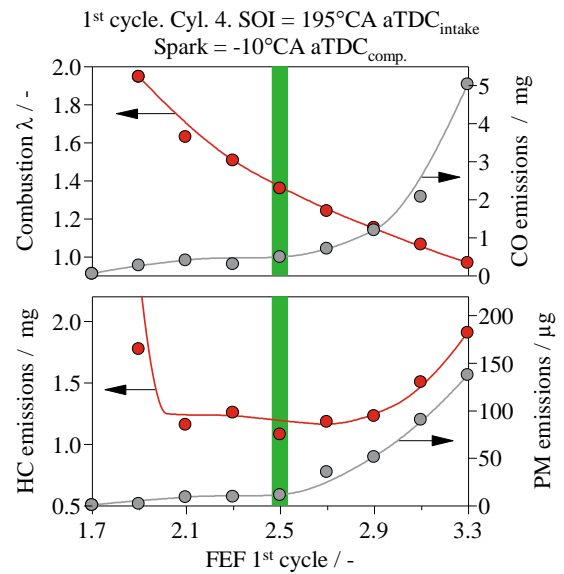


Figure 9. Calculated λ , CO, HC and PM emissions as a function of FEF_{1st} for the 1st cycle; λ calculated using the measured CO₂ and CO mole fractions

At FEF_{1st}=1.7 the resulting mixture is too lean and the cycle is a misfire. From FEF_{1st} =2.1 complete combustion takes place and the emissions plateau at 1.2 mg HC, 10 μ g PM and 0.4 mg CO. For FEF_{1st} greater than 2.7 all emissions increase rapidly, even though the overall λ of combustion (λ based on the exhaust CO and CO₂ values) is larger than 1.2. Based on these results FEF_{1st}=2.5 was selected as nominal 1st cycle FEF for further testing.

2nd and 3rd cycle dependence on FEF_{2nd} and FEF_{3rd}

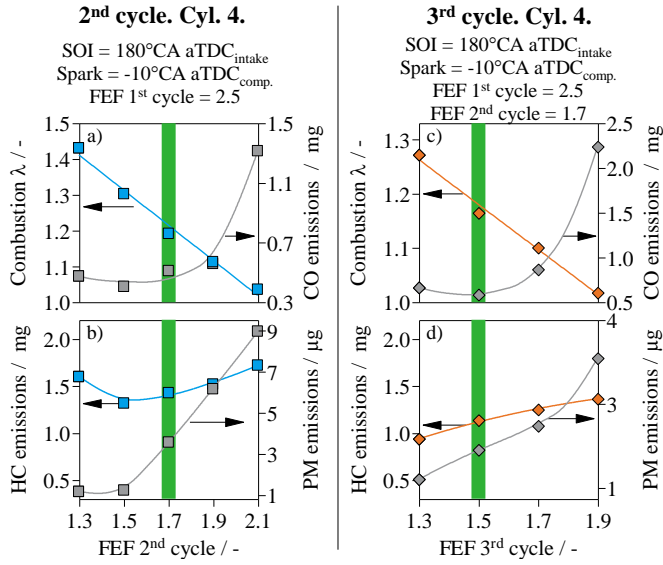


Figure 10. Values of λ , CO, HC and PM emissions as a function of FEF for the 2nd and 3rd cycle. The green band corresponds to the FEF selected for the subsequent SOI and spark timing sweep experiments

As it is the case with the 1st cycle, which is already discussed at the beginning of this section, the 2nd and 3rd cycle pollutant emissions are also dependent on the current cycle's FEF. Figure 10 shows combustion λ , CO, HC and PM emissions for the 2nd and 3rd cycles as a function of FEF. Both 2nd and 3rd cycles exhibit similarities in the trends. The combustion λ decreases linearly with FEF, and with similar slopes in both cases (increasing FEF by 0.2 would decrease combustion λ by approximately 0.1). As the combustion λ decreases to below 1.1, the CO emissions show a steep increase (Fig. 10-a and 10-c). The HC emissions show a slight increase with FEF; the 2nd and 3rd cycles HC emissions increase in 0.07 mg for an increase in 0.2 in FEF. The PM emissions also increase with FEF, although they exhibit different slopes for the 2nd and 3rd cycles. For a 0.2 increase in FEF, the 2nd cycle PM emissions increase in approximately 2.5 μg , while the 3rd cycle PM emissions do it in 0.7 μg .

The observed trends for the initial 3 cycles can be summarized as follows. For a 0.2 increase in FEF:

- 1st cycle: HC increase \sim 0.1 mg. PM increase \sim 30 μg
- 2nd cycle: HC increase \sim 0.07 mg. PM increase \sim 2.5 μg
- 3rd cycle: HC increase \sim 0.07 mg. PM increase \sim 0.7 μg

2nd cycle dependence on 1st cycle strategy

As can be inferred from the 1st cycle analysis in Fig. 9, more than half of the fuel injected in the 1st cycle does not participate in combustion. The remaining fuel is either pushed back into the intake manifold before IVC, absorbed into the lubricant oil, stored in the combustion chamber in the form of fuel films or lost to the crank-case in the form of blow-by gases. Some of this fuel will return to the cylinder, desorb from the oil layer or evaporate from the fuel films before the 2nd ignition event and participate in combustion. Given the importance of the residual fuel on the mixture formation process, it must be included in the analysis of the 2nd cycle FEF_{2nd} requirement. In a previous study

by the authors [10] the residual fuel available for combustion was quantified for the 2nd cycle by means of fuel carbon accounting using the HC exhausted from a non-firing 2nd cycle (see Fig. 11 bottom).

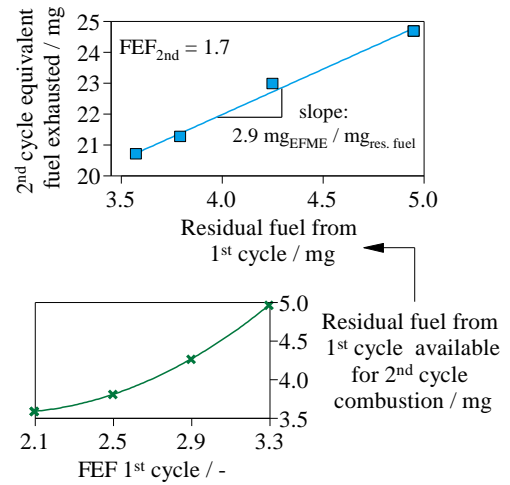


Figure 11. Top: 2nd cycle equivalent fuel mass exhausted as a function of the residual fuel for several 2nd cycle FEF_{2nd}. Bottom: Residual fuel from the 1st cycle as a function of the 1st cycle's FEF_{1st}.

The concept of the *equivalent fuel mass exhausted* (EFME) is introduced to facilitate the study of the impact that the residual fuel from the 1st cycle has on the mixture formation of the 2nd cycle. The EFME represents the amount of fuel necessary to produce the observed carbon mass exhausted, in the form of CO₂, CO and HC, in a given cycle (see Eq. 2).

$$EFME = m_{HC} + \frac{1}{x_{C,fuel}} \left(m_{CO_2} \frac{M_C}{M_{CO_2}} + m_{CO} \frac{M_C}{M_{CO}} \right) \quad (2)$$

Thus EFME represents the amount of fuel vapor available for combustion in the cycle.

Figure 11 (top) shows the EFME of the 2nd cycle as a function of the residual fuel for the case FEF_{2nd} = 1.7. The EFME increases linearly with the residual fuel. The resulting slope shows that an increase in 1 mg in residual fuel would result in an increase of 2.9 mg in EFME. The experiment was repeated at FEF_{2nd} values of 1.5, 1.9 and 2.1, and a similar slope was observed.

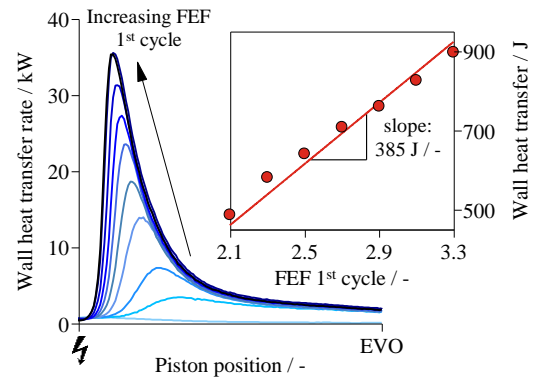


Figure 12. Wall heat transfer as a function of FEF_{1st} for the 1st cycle

That the increase of EFME is faster than the increase in residual fuel is explained as follows. The impact of the 1st cycle FEF_{1st} on the 2nd cycle mixture formation goes beyond the contribution of residual fuel from the 1st to the 2nd cycle. The 1st cycle fuel amount has a significant effect on the NIMEP_{1st} and on the combustion phasing at fixed spark timing [9]. As the heat release increases and is shifted to earlier points with higher 1st cycle FEF_{1st}, the wall heat transfer during the 1st cycle increases as well. Figure 12 shows the total wall heat transfer as a function of FEF_{1st} during the 1st cycle. The heat transfer rate was calculated using the Woschni [20] correlation corrected for low engine speeds [21].

The corresponding increase in cylinder wall temperature has an influence on the mixture formation process of the 2nd cycle, as it favors the evaporation of the injected fuel. In order to assess the impact of the wall heating during the 1st cycle on the 2nd cycle mixture formation, the effect of residual fuel is separated from that of wall heating via two sets of experiments:

1. 1st cycle wall heat transfer sweep, controlled with 1st cycle spark timing, at constant FEF_{1st} and residual fuel.
2. Residual fuel sweep at constant wall heat transfer in the first cycle. The procedure is achieved by suppressing the spark so that the 1st cycle does not fire; i.e. there is no combustion heat transfer.

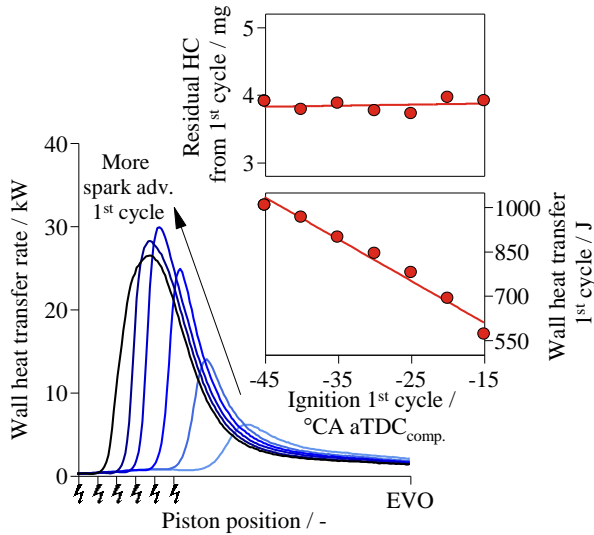


Figure 13. Wall heat transfer and residual fuel as a function of spark timing for the 1st cycle

For the first set of experiments, the wall heat transfer increases with spark advance; at the same time the residual fuel mass remains approximately unchanged; see Fig. 13. The spark timing sweep range was selected to achieve a similar heat transfer range as the one resulting from the 1st cycle FEF_{1st} sweep (Fig. 12). The dependence of the 2nd cycle equivalent fuel mass exhausted as a function of the 1st cycle total wall heat transfer for the case FEF_{2nd} = 1.7 is shown in Fig. 14. As the 1st cycle wall heat transfer is increased (through 1st cycle spark advance) the 2nd cycle EFME increases. Using a linear fit, the slope indicates that a 100 J increase in heat transfer would result in a 1mg increase in EFME. To further confirm the validity of these observations, the experiment was repeated at FEF_{2nd} values of 1.5, 1.9 and 2.1; similar dependences of the EFME on the 1st cycle heat transfer were observed.

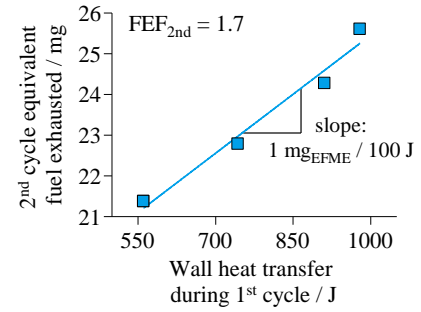


Figure 14. 2nd cycle equivalent fuel mass exhausted as a function of the wall heat transfer during the 1st cycle at constant residual fuel

For the second set of experiments, the 2nd cycle EFME as a function of the residual fuel, at constant 1st cycle wall heat transfer is shown in Fig. 15. The constant heat transfer condition was obtained by suppressing the ignition during the 1st cycle. In this way, the wall heat transfer is only a result of the mixture compression. The residual fuel range achieved with this approach is between 3.5 and 6.5 mg (Fig. 15 bottom). As shown in Fig. 15 (top), the increase in 2nd cycle EFME exhibits a monotonic trend with residual fuel. When the results are fitted linearly, the observed slope shows almost a 1-to-1 correspondence. Thus in the absence of change in wall temperature due to change in heat transfer, the increase in EFME corresponds to the increase in residual fuel from the previous cycle.

For consistency, the experiment was repeated at FEF_{2nd} values of 1.9 and 2.1, and a similar trend of 2nd cycle EFME against the residual fuel from the 1st cycle (constant 1st cycle heat transfer) was observed.

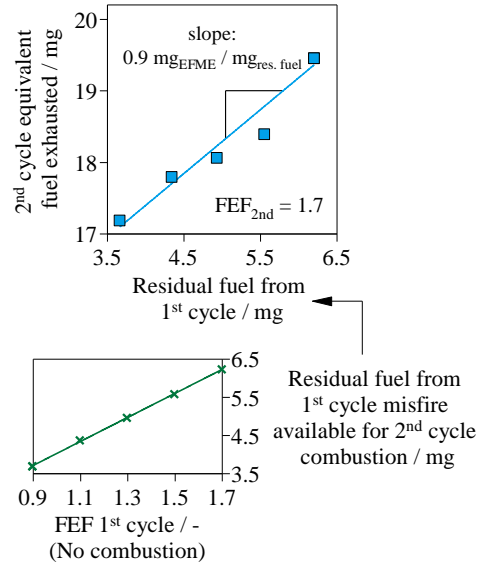


Figure 15. 2nd cycle equivalent fuel mass exhausted as a function of the residual fuel from the 1st cycle at constant heat transfer (1st cycle misfire)

The relative importance of the residual fuel and the wall heating effects on EFME of the 2nd cycle may be assessed as follows:

$$\Delta EFME = \frac{\partial EFME}{\partial m_R} \Delta m_R + \frac{\partial EFME}{\partial Q} \frac{\partial Q}{\partial FEF_{1st}} \Delta FEF_{1st} \quad (3)$$

Here m_R is the residual fuel mass from the 1st cycle and Q is the wall heat transfer in the 1st cycle. On the right-hand-side of Eq. (3), the first term represents the change of EFME in the second cycle due to the presence of the residual fuel from the first cycle; the second term represents the change of that due to the change in wall heat transfer in the first cycle.

The partial derivatives may be obtained from the experimental data:

- From Fig. 15, $\frac{\partial EFME}{\partial m_R} = 0.9$
- From Fig. 14, $\frac{\partial EFME}{\partial Q} = 10^{-2} \text{ mg/J}$
- From Fig. 12, $\frac{\partial EFME}{\partial FEF_{1st}} = 385 \text{ J}$

For the data shown in Fig. 11, for a change of 1st cycle FEF_{1st} from 2.1 to 3.3 ($\Delta FEF_{1st} = 1.2$), m_R increases from 3.6 to 4.95 mg ($\Delta m_R = 1.35 \text{ mg}$). Then numerical values for Eq. (3) become:

$$\Delta EFME = 1.22 \text{ mg} + 4.62 \text{ mg} = 5.84 \text{ mg} \quad (4)$$

The above value is in line with the observed value of $\Delta EFME = 4.1 \text{ mg}$ in Fig. 11. More importantly, Eq. (4) shows that the effect of the change of the wall heat transfer in the 1st cycle on the second cycle EFME is approximately 4 times that of the residual fuel amount.

Start of Injection (SOI) effect

The injection timing is an important parameter for the GDI cold-start calibration. The effect of SOI on the mixture formation process and engine out emission has been studied in the past for the 1st combustion cycle [9] and for the cold fast-idle period [22, 23]. In this section the analysis is extended to the 2nd and 3rd cycles. The FEF and spark timing were held constant for each cycle as well as the SOI of the preceding cycles. The relevant experimental parameters used can be found in Table 3. The choice of these values would give good HC and PM emissions for the reference cases; see Fig. 9 and 10.

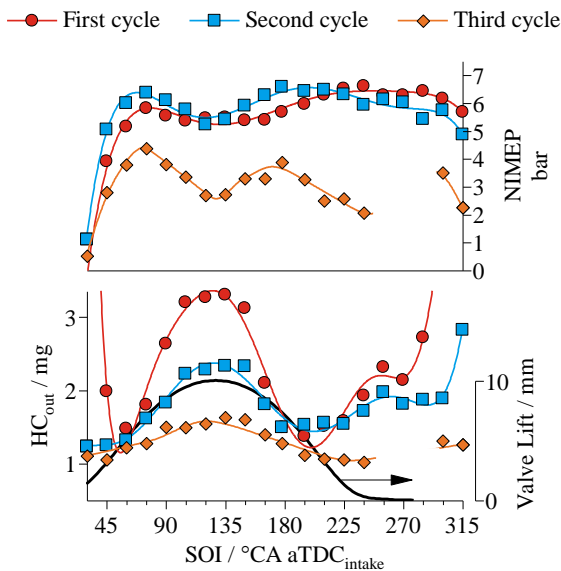


Figure 16. NIMEP and HC emissions as a function of SOI for the 1st, 2nd and 3rd cycles during crank-start

Table 3. Start of injection sweep parameters for the 1st, 2nd, and 3rd cycles

| Parameter | 1 st cycle | 2 nd cycle | 3 rd cycle |
|--|-----------------------|-----------------------|-----------------------|
| FEF / - | 2.5 | 1.7 | 1.5 |
| Fuel mass / mg | 74 | 44 | 32 |
| Injection duration / °CA | 11 | 15 | 16 |
| Spark timing / °CA aTDC _{comp.} | -10 | -10 | -10 |
| SOI (previous cycles) / °CA aTDC _{intake} | 180 | 180 | - |

The NIMEP and HC emissions as a function of the injection timing are shown in Fig. 16 for the initial 3 cycles. The trends observed in the SOI sweeps are similar in shape for the initial 3 cycles, although the magnitudes differ. The following discussion applies to all 3 cycles studied. Injection timings earlier than $SOI = 45^\circ\text{CA aTDC}_{intake}$ cause significant piston impingement and poor mixture formation. As SOI is retarded the piston impingement is reduced, favoring the mixture preparation and resulting in a sharp increase in NIMEP. At $SOI = 75^\circ\text{CA aTDC}_{intake}$ the NIMEP reaches a local maximum and the HC emissions start to increase rapidly. From $SOI = 75$ to $180^\circ\text{CA aTDC}_{intake}$ the interaction between the injection spray and the intake valve has a noticeable effect on the NIMEP and HC emissions. The intake valve lift profile is shown in Fig. 16 (bottom). The maximum intake valve lift corresponds with a local minimum in NIMEP and a local maximum in HC emissions. However, as the crank-start progresses from the 1st to the 3rd cycle, the spray/valve interaction has a diminishing impact on HC emissions and an increasing effect on NIMEP (see Table 4).

Table 4. Effect of spray/valve interaction on NIMEP and HC emissions for the initial 3 cycles.

| Parameter | 1 st cycle | 2 nd cycle | 3 rd cycle |
|--|-----------------------|-----------------------|-----------------------|
| NIMEP @ $SOI = 75^\circ\text{CA aTDC}_{intake}$ | 5.8 bar | 6.4 bar | 4.4 bar |
| NIMEP @ $SOI = 120^\circ\text{CA aTDC}_{intake}$ | 5.4 bar | 5.2 bar | 2.7 bar |
| NIMEP reduction | -7 % | -19 % | -39 % |
| HC @ $SOI = 60^\circ\text{CA aTDC}_{intake}$ | 1.5 mg | 1.3 mg | 1.2 mg |
| HC @ $SOI = 120^\circ\text{CA aTDC}_{intake}$ | 3.3 mg | 2.3 mg | 1.6 mg |
| HC emissions increase | +120 % | +77 % | +33 % |

Injection timings in the initial part of the compression stroke, where the intake valve lift is lower than 6 mm, result in a flat region of low HC emissions. As the SOI is further delayed between 240 and $300^\circ\text{CA aTDC}_{intake}$, the HC emissions increase due to the decay in turbulence intensity and its negative effect on mixture formation [22]. In the case of the 3rd cycle, the engine misfired and the results are not reported. After $SOI=300^\circ\text{CA aTDC}_{intake}$, the spray/piston interaction results in mixture stratification in the vicinity of the spark plug, enabling robust combustion but with an increase in HC emissions.

Figure 17 shows the PM/PN emissions as a function of the SOI for the initial 3 cycles. Common to all 3 cycles, injection timings in the first half of the intake stroke result in higher PM/PN emissions in comparison to SOI in the late intake stroke. In contrast to the HC emissions, the interaction between the injection spray and the intake valve leads to a reduction in PM emissions. In the case of the 1st cycle, the minimum PM/PN emissions are achieved for SOI during the early compression stroke. After this point the PM emissions increase monotonically with SOI retard, mainly due to interaction with the piston. The 2nd cycle PM/PN dependence on SOI shows a similar behavior. The SOI for minimum PM/PN is located in the region of

maximum intake valve lift, at approximately $\text{SOI}=135^\circ\text{CA aTDC}_{\text{intake}}$. After this point, the decrease in turbulence intensity and the interaction with the piston crown drives the PM/PN emissions up. Lastly, the 3rd cycle SOI sweep features a region of constant PM emissions for SOI between 120 and $225^\circ\text{CA aTDC}_{\text{intake}}$.

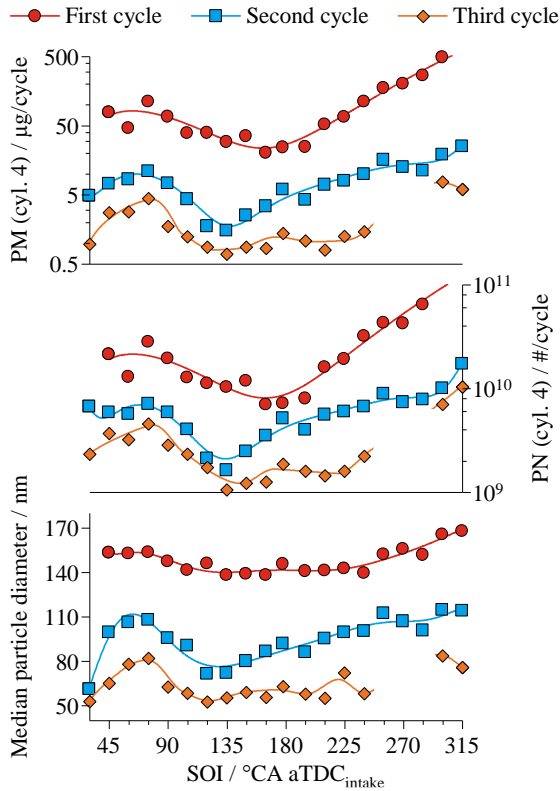


Figure 17. PM emissions and median particle diameter as a function of CA50 for the 1st, 2nd and 3rd cycles during crank-start

The changes observed in PM emissions with SOI and cycle number are significant, covering orders of magnitude. The observed increase in PM with SOI retard is driven by the increase in particle nucleation (PN emissions). The reduction in PM from the 1st to the 3rd cycle is a result of both lower particle nucleation and reduced agglomeration rate (smaller particle size).

Combustion phasing effect

The use of retarded spark timing during the cold fast-idle period (first 20 sec. of FTP-75) is a common strategy in the cold-start calibration of LDVs [24] for accelerating the catalyst light-off time and reducing the engine-out HC emissions. The reduction in HC emissions with spark retard is mainly associated with the in-cylinder consumption of the fresh mixture stored in the crevice volumes by the flame, with post-flame and exhaust runner oxidation playing less important roles [25]. During the cold crank-start of GDI engines, the significant over-fueling necessary to form a combustible mixture results in the formation of fuel films. The liquid fuel films become a dominant source for HC emissions, comparable to or greater than the crevice storage mechanism [7]. Higher burned gas temperatures in the expansion process with retarded timing promotes both the evaporation and oxidation of the HC contained in the fuel films. Thus, the impact of late combustion phasing on crank-start HC emissions is not straight forward.

Table 5. Spark timing sweep parameters for the 1st, 2nd, and 3rd cycles

| Parameter | 1 st cycle | 2 nd cycle | 3 rd cycle |
|--|-----------------------|-----------------------|-----------------------|
| FEF / - | 2.5 | 1.7 | 1.5 |
| Fuel mass / mg | 74 | 44 | 32 |
| SOI / °CA aTDC _{intake} | 195 | 180 | 180 |
| CA50 (previous cycles) / °CA aTDC _{comp.} | 10 | 17 | - |

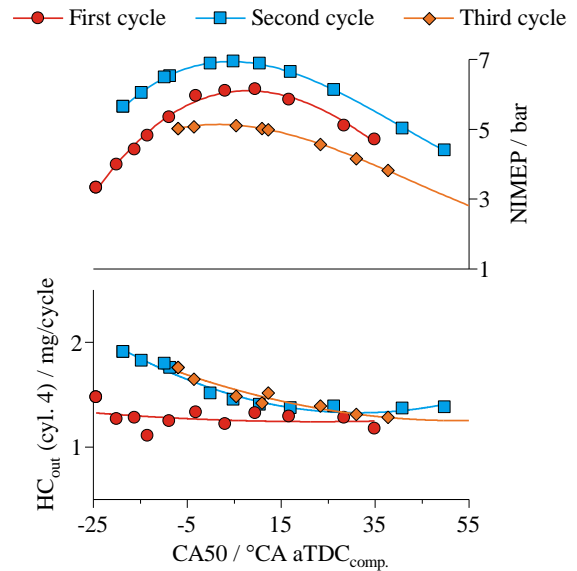


Figure 18. NIMEP and HC emissions as a function of CA50 for the 1st, 2nd and 3rd cycles during crank-start

Figures 18 and 19 show the dependence of NIMEP, HC and PM emissions on the combustion phasing, quantified by the point for 50% of heat release (CA50). The FEF and SOI were held constant for each cycle; the CA50 of the preceding cycles were also held constant (see Table 5). The selection of the nominal FEF and SOI for each cycle was based on the emissions and NIMEP trends presented on the preceding sections.

Due to the low engine speed and the rapid change in speed during crank-start, especially for the 1st cycle, the usual notion of combustion phasing for MBT ($\text{CA50} \sim 7^\circ \text{aTDC}_{\text{comp.}}$) does not apply [26]. Figure 18 (top) shows the NIMEP as a function of CA50 for the first 3 cycles. The maximum NIMEP is achieved at $\text{CA50} \sim 10^\circ \text{aTDC}_{\text{comp.}}$ for the 1st cycle, and at $\text{CA50} \sim 5^\circ \text{aTDC}_{\text{comp.}}$ for the 2nd and 3rd cycles.

The HC emissions of the 1st cycle are insensitive to combustion phasing, the values remain constant at 1.3 mg/cyl./cycle for the entire sweep. This observation suggests that the 1st cycle HC emissions predominantly derive from the liquid film. Unlike the crevice stored HC, the fuel vapor from liquid films is not premixed with air, and its oxidation is less sensitive to increased post-flame temperatures associated with the combustion retard. In contrast, the HC emissions for the 2nd and 3rd cycles are reduced with later combustion phasing, undergoing a 30% reduction for the range of combustion phasing delay in this study. The observation suggests an increasing importance of the crevice mechanism as the liquid film is much reduced in the 2nd and 3rd cycle.

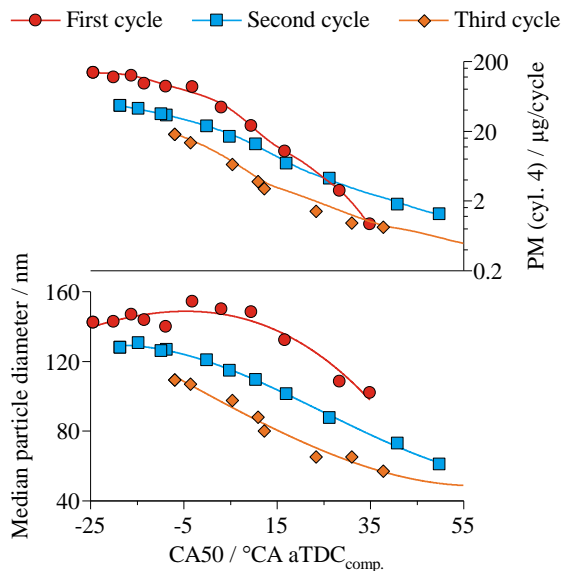


Figure 19. PM emissions and median particle diameter as a function of CA50 for the 1st, 2nd and 3rd cycles during crank-start

The PM/PN emissions as a function of combustion phasing are presented in Fig. 19. The formation of the particulates is driven by the pyrolysis of the fuel rich mixture created by evaporation of the liquid fuel films [22]. As combustion is delayed, the time available for the mixing of the vapor originating from the liquid fuel films increases while the time for particulate nucleation through fuel vapor pyrolysis and accumulation through HC condensation is reduced. As a result, for each of the 3 cycles studied the PM is reduced by more than one order of magnitude with late combustion phasing, due to lower particulate number and smaller median particulate size.

Conclusions

The effects of fuel amount, injection timing and spark timing on the HC and PM emissions of the first 3 cycles during cold crank-start (20°C) were studied in a wall guided gasoline direct injection engine. The main results can be summarized as follows:

1. The adverse conditions of low temperature and limited charge motion (because of the low speed) during cold crank-start result in mixture inhomogeneity. Consequently, aiming for an overall combustion λ of 1 is not a viable strategy as it increases the CO, HC and PM emissions. The amount of fuel injected needs to be large enough to reduce the risk of misfire or partial burn, and sufficiently small to control the engine out emissions. The results show that the optimum fuel enrichment factor (FEF) for the initial 3 cycles are $FEF_{1st} = 2.5$, $FEF_{2nd} = 1.7$ and $FEF_{3rd} = 1.5$.
2. For the range of FEF studied, the HC emissions for the initial 3 cycles are of the same order of magnitude; between 1 and 1.5 mg/cyl./cycle. In contrast, the PM emissions per cycle are reduced by more than an order of magnitude as the crank-start progresses from the 1st to the 3rd cycle.
3. The FEF history has an influence on the mixture formation through two mechanisms. First, as the FEF of previous cycle increases, so does the residual fuel mass. Second, the amount

and point of heat release for the previous cycles is a function of FEF. The heat release increase of the previous cycles translates into wall heating, impacting the fuel evaporation and mixture formation process of the current cycle. The effect of wall heating is estimated to be approximately 4 times that of the residual fuel mass on the amount of combustible fuel vapor prepared in the current cycle.

4. The SOI selection for minimizing the pollutant emissions presents a tradeoff. The lowest HC emissions are achieved for SOI during the first half of the intake stroke, for intake valve lifts lower than 5 mm. Contrary, the minimum PM emissions are achieved for SOI during the intake stroke with the intake valve lift greater than 5 mm. Injection during the early compression stroke results in a good compromise for both HC and PM emissions.
5. The effect of fuel spray interaction with the intake valve on HC emissions is reduced as the crank-start progresses from the 1st to the 3rd cycle because less fuel is injected in the later cycles.
6. The HC emissions of the 1st cycle are insensitive to combustion phasing. For the 2nd and 3rd cycles, spark timing retard results in approximately a 30% reduction as CA50 goes from -10 to 30° aTDC_{comp.}. For the 3 cycles studied, the observed PM reduction with combustion retard is larger than an order of magnitude as CA50 goes from -10 to 30° aTDC_{comp.}.

References

1. Façanha, Cristiano, Kate Blumber, and Josh Miller. "Global Transportation Energy and Climate Roadmap." International Council on Clean Transportation, 2012.
2. EPA; NHTSA. "Final Rulemaking for 2017-2025 Light-Duty Vehicle Greenhouse Gas Emission Standards and Corporate Average Fuel Economy Standards." 2012.
3. Davis, Stacy, Susan Diegel, Ridge Boundy, and Sheila Moore. "Vehicle Technologies Market Report 2014." Oak Ridge National Laboratory, 2015
4. "European Vehicle Market Statistics, 2014." International Council on Clean Transportation, 2014.
5. Chen, Hai-Ying, and Hsiao-Lan (Russell) Chang. "Development of Low Temperature Three-Way Catalysts for Future Fuel Efficient Vehicles." *Johnson Matthey Technology Review* 59, no. 1 (January 1, 2015): 64–67. doi:10.1595/205651315X686011.
6. Myung, Cha-Lee, Juwon Kim, Wonwook Jang, Dongyoung Jin, Simsoo Park, and Jeongmin Lee. "Nanoparticle Filtration Characteristics of Advanced Metal Foam Media for a Spark Ignition Direct Injection Engine in Steady Engine Operating Conditions and Vehicle Test Modes." *Energies* 8, no. 3 (March 9, 2015): 1865–81. doi:10.3390/en8031865.
7. Costanzo, Vincent S., and John B. Heywood. "Effect of In-Cylinder Liquid Fuel Films on Engine-Out Unburned Hydrocarbon Emissions for an SI Engine," SAE Technical Paper 2012-01-1712, 2012. doi:10.4271/2012-01-1712.
8. Cheng, Wai K., Douglas Hamrin, John B. Heywood, Simone Hochgreb, Kyoungdoug Min, and Michael Norris. "An Overview of Hydrocarbon Emissions Mechanisms in Spark-Ignition Engines," SAE Technical Paper 932708, 1993. doi:10.4271/932708.
9. Rodriguez, J. Felipe, and Wai K. Cheng. "Effect of Operation Strategy on First Cycle CO, HC, and PM/PN Emissions in a GDI

- Engine.” *SAE International Journal of Engines* 8, no. 3 (April 14, 2015). doi:10.4271/2015-01-0887.
10. Rodriguez, J. Felipe, and Wai K. Cheng. “Fuel Carbon Pathway in the First Cranking Cycle of a Gasoline Direct Injection Engine.” *International Journal of Engine Research*, October 5, 2015. doi:10.1177/1468087415609852.
 11. Cheng, Wai K., and Fuquan Zhao. “Transient Engine Startup and Shutdown Processes.” In *Technologies for Near-Zero-Emission Gasoline-Powered Vehicles*, 1–29. SAE International, 2006.
 12. Lang, Kevin R., Wai K. Cheng, Mark Borland, Chris Thomas, and Fuquan Zhao. “Effect of Intake Cam Phasing on First Cycle Fuel Delivery and HC Emissions in an SI Engine.” SAE Technical Paper 2004-01-1852, 2004. doi:10.4271/2004-01-1852.
 13. Lang, K. and Wai K. Cheng, "Effect of Fuel Properties on First Cycle Fuel Delivery in a SI Engine," SAE Technical Paper 2004-01-3057, 2004. doi:10.4271/2004-01-3057.
 14. Cowart, J., "Air-Fuel Ratio Measurement Diagnostics During Cranking and Startup in a Port-Fuel-Injected Spark-Ignition Engine," SAE Technical Paper 2004-01-1915, 2004. doi:10.4271/2004-01-1915.
 15. Santoso, H. and Wai K. Cheng, "Mixture Preparation and Hydrocarbon Emissions Behaviors in the First Cycle of SI Engine Cranking," SAE Technical Paper 2002-01-2805, 2002. doi:10.4271/2002-01-2805.
 16. Klein, D. and Wai K. Cheng, "Spark Ignition Engine Hydrocarbon Emissions Behaviors in Stopping and Restarting," SAE Technical Paper 2002-01-2804, 2002. doi:10.4271/2002-01-2804.
 17. Chen, Kuo Chiang, Wai K. Cheng, Jane M. Van Doren, James P. Murphy, Matthew D. Hargus, and Sarah A. McSweeney. “Time-Resolved, Speciated Emissions from an SI Engine During Starting and Warm-Up,” SAE Technical Paper 961955, 1996. doi:10.4271/961955.
 18. Burke, David, David Foti, James Haller, and William J. Fedor. “Fuel Rail Pressure Rise during Cold Start of a Gasoline Direct Injection Engine,” SAE Technical Paper 2012-01-0393, 2012. doi:10.4271/2012-01-0393.
 19. Tang, Huayin, Richard Burke, Sam Akehurst, Chris Brace, et al. “Behaviours of a GDI Gasoline Engine during Start,” SAE Technical Paper 2014-01-1374, 2014. doi:10.4271/2014-01-1374.
 20. Woschni, G. “A Universally Applicable Equation for the Instantaneous Heat Transfer Coefficient in the Internal Combustion Engine,” SAE Technical Paper 670931, 1967. doi:10.4271/670931.
 21. Lejsek, David, Andre Kulzer, Günter Hohenberg, and Michael Bargende. “Novel Transient Wall Heat Transfer Approach for the Start-up of SI Engines with Gasoline Direct Injection.” *SAE International Journal of Engines* 3, no. 1 (April 12, 2010): 1053–70. doi:10.4271/2010-01-1270.
 22. Ketterer, Justin E., and Wai K. Cheng. “On the Nature of Particulate Emissions from DISI Engines at Cold-Fast-Idle.” *SAE International Journal of Engines* 7, no. 2 (April 1, 2014): 986–94. doi:10.4271/2014-01-1368.
 23. Cedrone, Kevin, and Wai K. Cheng. “SI Engine Control in the Cold-Fast-Idle Period for Low HC Emissions and Fast Catalyst Light Off.” *SAE International Journal of Engines* 7, no. 2 (April 1, 2014): 968–76. doi:10.4271/2014-01-1366.
 24. Ball, Douglas, Corey Negohosian, Deven Ross, David Moser, and Richard McClaughry. “Comparison of Cold Start Calibrations, Vehicle Hardware and Catalyst Architecture of 4-Cylinder Turbocharged Vehicles.” *SAE International Journal of Engines* 6, no. 4 (October 14, 2013): 1922–33. doi:10.4271/2013-01-2593.
 25. Eng, James A. “The Effect of Spark Retard on Engine-out Hydrocarbon Emissions,” SAE Technical Paper 2005-01-3867, 2005. doi:10.4271/2005-01-3867.
 26. Cheng, Wai K., and Fuquan Zhao. “Transient Engine Startup and Shutdown Processes.” In *Technologies for Near-Zero-Emission Gasoline-Powered Vehicles*, 1–29. SAE International, 2006.

Contact Information

Felipe Rodríguez, jfrib@mit.edu

Wai Cheng, wkcheng@mit.edu

Acknowledgments

The authors would like to acknowledge the support for this research by Borg-Warner, Fiat Chrysler Automobiles, Ford Motor Company, and General Motors Company through a Consortium on Engine and Fuels Research.

Abbreviations

| | |
|-------------------------------|---|
| AFR | Air Fuel Ratio |
| aTDC_{comp} | After Top Dead Center Compression |
| aTDC_{intake} | After Top Dead Center Intake |
| BDC | Bottom Dead Center |
| CA50 | Point for 50% of heat release |
| CMD | Count Median Diameter |
| DMS | Differential Mobility Spectrometer |
| EFME | Equivalent Fuel Mass Exhausted; see Eq. (2) |
| EGSS | Exhaust Gas Sampling System |
| FEF | Fuel Enrichment Factor; see Eq. (1) |
| FFID | Fast Flame Ionization Detector |
| FTP | Federal Test Procedure |
| (F/A)_{stoich} | Stoichiometric fuel air ratio |
| GDI | Gasoline Direct Injection |
| GPF | Gasoline Particle Filter |
| IVC | Intake Valve Closing |
| IVO | Intake Valve Opening |
| LDV | Light Duty Vehicle |
| MAP | Manifold Absolute Pressure |
| MBT | Maximum Brake Torque |
| m_{f,cyl} | Injected fuel mass per cylinder |
| m_y | Mass exhausted of species y |
| M_y | Molecular weight of species y |
| NDIR | Non-Dispersive Infrared sensor |

| | | | |
|--------------|---------------------------------------|--------------|------------------------------|
| NEDC | New European Driving Cycle | TDC | Top Dead Center |
| NIMEP | Net Indicated Mean Effective Pressure | $x_{C,fuel}$ | Carbon mass fraction of fuel |
| PM | Particulate Mass | η_{vol} | Volumetric efficiency |
| PN | Particulate Number | γ | Heat capacity ratio |
| SOI | Start of Injection | ρ_{int} | Intake air density |
| V_{cyl} | Cylinder volume | | |
| TWC | Three Way Catalyst | | |